HHS Public Access

Author manuscript

Nat Med. Author manuscript; available in PMC 2019 September 04.

Published in final edited form as:

Nat Med. 2019 April ; 25(4): 620–627. doi:10.1038/s41591-019-0367-9.

Protective autophagy elicited by RAF→MEK→ERK inhibition suggests a treatment strategy for RAS-driven cancers

Conan G. Kinsey[1,2], **Soledad A. Camolotto**[1], **Amelie M. Boespflug**[1,3,4], **Katrin P. Gullien**[1], **Mona Foth**[1], **Amanda Truong**[1], **Sophia S. Schuman**[1], **Jill E. Shea**[5], **Michael T. Seipp**[5], **Jeffrey T. Yap**[1,6], **Lance D. Burrell**[1], **David H. Lum**[1], **Jonathan R. Whisenant**[1,2], **G. Weldon Gilcrease III**[1,2], **Courtney C. Cavalieri**[1,7], **Kaitrin M. Rehbein**[1], **Stephanie L. Cutler**[1], **Kajsa E. Affolter**[1,8], **Alana L. Welm**[1,9], **Bryan E. Welm**[1,5], **Courtney L. Scaife**[1,5], **Eric L. Snyder**[1,8], and **Martin McMahon**[1,10,*]

[1.]Huntsman Cancer Institute, University of Utah, 2000 Circle of Hope, Salt Lake City, UT 84112, USA

[2.]Department of Internal Medicine, Division of Oncology, University of Utah School of Medicine, 30 North 1900 East, Salt Lake City, Utah 84132

[3.]Department of Dermatology, Centre Hospitalier Lyon-Sud, 165 Chemin du Grand Revoyet 69495 Pierre Benite, Cedex, France

[4.]Cancer Research Center of Lyon, Claude Bernard Lyon-1 University, INSERM 1052, CNRS 5286

[5.]Department of Surgery, University of Utah School of Medicine 30 North 1900 East, Salt Lake City, Utah 84132

[6.]Department of Radiology and Imaging Services, University of Utah School of Medicine 30 North 1900 East, Salt Lake City, Utah 84132

[7.]Department of Pharmacy Services, Huntsman Cancer Institute, University of Utah, 2000 Circle of Hope, Salt Lake City, UT 84112, USA

[8.]Department of Pathology, University of Utah School of Medicine, 15 North Medical Drive East, Salt Lake City, Utah 84112

[9.]Department of Oncological Sciences, University of Utah School of Medicine 30 North 1900 East, Salt Lake City, Utah 84132

[*]**Corresponding author:** Department of Dermatology & Huntsman Cancer Institute, University of Utah, 2000 Circle of Hope, Salt Lake City, UT 84112, (801) 213 5790, martin.mcmahon@hci.utah.edu.

Author Contributions:

C.G.K. and M.M designed all experiments. C.G.K., S.A.C., A.M.B., K.P.G., M.F., A.T. and S.S.S. performed *in vitro* and *in vivo* experiments and collected data. J.T.Y. and L.D.B. designed, performed and analyzed *in vivo* FDG-PET/MRI/CT imaging studies. J.E.S., M.T.S., D.H.L, A.L.W., B.E.W., and C.L.S established, maintained and provided PDX mouse models. C.G.K., J.R.W., G.W.G., C.C.C., K.M.R., and S.L.C. provided patient care. K.E.A. assisted with pathologic analysis of samples. C.G.K. and M.M. analyzed data, prepared the manuscript and guided the manuscript through review.

Competing Interests Statement:

Dr. McMahon served on external advisory boards for Novartis (June 2017), Genentech (December 2017) and Merck (June 2018). Dr. McMahon is the recipient of research funding from Pfizer, through a grant peer-reviewed, co-funded and awarded by the Melanoma Research Alliance.

[10]Department of Dermatology, University of Utah School of Medicine, 30 North 1900 East, Salt Lake City, Utah 84132

INTRODUCTION

Pancreatic ductal adenocarcinoma (PDA) was responsible for ~44,000 deaths in the USA in 2018, and is the epitome of a recalcitrant cancer driven by a pharmacologically intractable oncoprotein, KRAS [1–4]. Downstream of KRAS, the RAF→MEK→ERK signaling pathway plays a central role in pancreatic carcinogenesis [5]. However, paradoxically, inhibition of this pathway has provided no clinical benefit to PDA patients [6]. Here we show that inhibition of KRAS→RAF→MEK→ERK signaling elicits autophagy, a process of cellular recycling that protects PDA cells from the cytotoxic effects of KRAS pathway inhibition. Mechanistically, inhibition of MEK1/2 leads to activation of the LKB1→AMPK→ULK1 signaling axis, a key regulator of autophagy. Furthermore, combined inhibition of MEK1/2 plus autophagy displays synergistic anti-proliferative effects against PDA cell lines *in vitro*, and promotes regression of xenografted patient-derived PDA tumors in mice. The observed effect of combination trametinib plus chloroquine was not restricted to PDA as other tumors, including patient-derived xenografts (PDX) of *NRAS*-mutated melanoma and *BRAF*-mutated colorectal cancer displayed similar responses. Finally, treatment of a PDA patient with the combination of trametinib plus hydroxychloroquine resulted in a partial, but nonetheless striking disease response. These data suggest that this combination therapy may represent a novel strategy to target RAS-driven cancers.

RESULTS

Increased autophagic flux in response to inhibition of KRAS→RAF→MEK→ERK signaling.

To test the hypothesis that RAF→MEK→ERK signaling may regulate autophagic flux in PDA cells, we tested the consequences of targeted inhibition of this pathway in MIA-PaCa2 ($KRAS^{G12C}$), BxPC3 ($BRAF^{\Delta V487\text{-}P492}$) and PDX220 ($KRAS^{G12V}$) PDA cells, the last derived from a *KRAS*-mutated PDA PDX. PDA cells were engineered to express a chimaeric autophagic flux reporter protein consisting of: mCherry, GFP and LC3 (AFR, Fig. 1a) [7]. The LC3 component targets the chimaera to the autophagosome, the mCherry component contributes a pH insensitive red fluorescence, and the GFP component contributes a pH sensitive green fluorescence that is diminished in the low pH (≤5) environment of the autophagosome and lysosome. Hence, the ratio of mCherry:GFP fluorescence is a measure of autophagic flux in these cells (Fig. 1a, Ext. Fig 1) [8].

Treatment of Mia-PaCa2^{AFR} cells with temsirolimus, an mTORC1 inhibitor, led to the expected increase in the mCherry:GFP fluorescence ratio (Fig. 1b, Ext. Fig. 1d). By contrast, treatment of Mia-PaCa2^{AFR} cells with either chloroquine (CQ) or SAR-405, an inhibitor of the class III PI3'-kinase VPS34, led to the expected decrease in the mCherry:GFP fluorescence ratio (Fig. 1b, Ext. Figs. 1b-c) [9, 10]. Next, Mia-PaCa2^{AFR} cells were treated with inhibitors of $KRAS^{G12C}$→RAF→MEK→ERK signaling including: ARS-853 (covalent inhibitor of $KRAS^{G12C}$), trametinib or cobimetinib (MEK1/2 inhibitors), or

SCH772984 (ERK1/2 inhibitor) (Figs. 1c-f) [11–15]. All of these inhbitors increased the mCherry:GFP fluorescence ratio indicating that blockade of multiple nodes of $KRAS^{G12C}$→RAF→MEK→ERK signaling led to increased autophagic flux. Confirmation of increased autophagic flux was obtained by immunoblotting of extracts of trametinib-treated Mia-PaCa2 cells for the degradation p62 and the conversion of LC3-I to LC3-II by the covalent conjugation of phosphatidylethanolamine, (Ext. Figs. 2a,c). To extend these observations $BxPC3^{AFR}$ and $PDX220^{AFR}$ cells were treated with trametinib, which also led to a readily detected increase in autophagic flux (Figs. 1g-h, Ext. Fig 2b).

Trametinib-induced autophagic flux is mediated by the LKB1→AMPK→ULK1/ATG1 signaling axis.

To determine the mechanism(s) by which inhibition of $KRAS^{G12C}$→RAF→MEK→ERK signaling promotes autophagic flux, Mia-PaCa2 cells were treated with different concentrations of trametinib for 48 hours or PDX220 cells were treated with trametinib (100nM) over a time course with the expression or phosphorylation of potential downstream mediators of autophagy assessed by immunoblotting (Figs. 1i-j). Previous work indicated that ERK1/2 can inhibit LKB1 through phosphorylation of serine 428 (pS428) [16]. LKB1 in turn acts upstream of the AMPK→ULK1/ATG1 signaling axis to regulate autophagy [17, 18]. Consistent with this, inhibition of MEK→ERK signaling in Mia-PaCa2 or PDX220 cells led to decreased phosphorylation of pS428-LKB1 and increased phosphorylation of AMPK (pT172) and ULK1 (pS555). Consistent with these observations, either shRNA-mediated inhibition of LKB1 expression or ectopic expression of dominant-negative $AMPK^{K45R}$ or $ULK1^{M92A}$ significantly attenuated, but did not fully abrogate, trametinib-induced autophagy (Figs. 1l-m, Ext. Figs. 2d &e). Hence, these data are consistent with the hypothesis that trametinib-induced autophagy in PDA cell lines is mediated, at least in part, by increased flux through the LKB1→AMPK→ULK1/ATG1 signaling axis (Fig. 1k) [19].

Trametinib and chloroquine are synergistically cytotoxic to PDA cell lines *in vitro*.

Despite the central role of the RAF→MEK→ERK MAP kinase signaling in PDA, MEK1/2 inhibitors have failed to display clinical benefit in PDA patients [9, 10]. Hence, we hypothesized that trametinib-induced autophagic flux may serve as a protective mechanism for the survival of PDA cells in the face of RAF→MEK→ERK pathway inhibition. To test this, Mia-PaCa2, BxPC3 or PDX220 cells were treated with different concentrations of trametinib or chloroquine, either alone or in combination, with drug synergy/antagonism assessed by the Loewe Additivity method (Fig. 2a) [20]. Consistent with our hypothesis, we observed synergistic anti-proliferative effects at chloroquine concentrations in the range of 12.5–25μM when combined with trametinib in the range of 8–200nM (Fig. 2a). Additionally, treatment with trametinib plus chloroquine resulted in increased caspase 3/7 activation and increased cumulative cell death compared to the single agents, suggesting cooperative activation of apoptotic cell death (Figs. 2b-d). These data are consistent with our model that trametinib-induced autophagic flux serves to protect PDA cells from the potentially pro-apoptotic effects of RAF→MEK→ERK pathway inhibition.

Dominant-negative ATG4B^{DN} combined with trametinib promotes regression of established MIA-PaCa2 xenografts.

4-aminoquinolones such as chloroquine and hydroxychloroquine are pleiotropic such that, in addition to inhibiting autophagy, they have effects on macro- and micropinocytosis, mitochondrial function and other processes [21, 22]. We therefore wished to determine whether the cooperative effects of trametinib plus chloroquine could be ascribed, at least in part, to autophagy inhibition. To address this, we expressed a dominant-negative (DN) form of ATG4B (ATG4B^{C74A}, ATG4B^{DN}) under the control of a tetracycline-regulated promoter in Mia-PaCa2^{AFR} cells (Mia-PaCa2^{AFR}-ATG4B^{DN} cells). Consistent with its ability to inhibit autophagy [23, 24], expression of ATG4B^{DN} inhibited the trametinib-induced autophagic flux observed in Mia-PaCa2^{AFR} cells as assessed by flow cytometry or immunoblotting for p62 abundance or LC3 processing (Figs. 3a-b). Next, tumors generated by xenografting Mia-PaCa2^{AFR}-ATG4B^{DN} cells into NOD/SCID mice were treated with: 1. vehicle control; 2. Doxycycline (to induce ATG4B^{DN}); 3. trametinib (1mg/kg, q.d.) or; 4. the combination of doxycycline plus trametinib. Whereas trametinib treatment had a modest cytostatic effect, expression of ATG4B^{DN} had no detectable effect on tumor growth. However, expression of ATG4B^{DN} in the presence of trametinib led to regression of established tumors (Fig. 3c). Immunohistochemical analysis of tumor sections revealed decreased pERK1/2 in tumors from trametinib treated mice and elevated expression of ATG4B^{DN} in tumors from doxycycline treated mice. Importantly, tumors from trametinib treated mice displayed reduced abundance of p62, consistent with increased autophagic flux. However, p62 expression was greatly increased when autophagic flux was inhibited by ATG4B^{DN} expression (Fig. 3d). These data indicate that, in a tumor cell autonomous manner, ATG4B^{DN}-mediated inhibition of autophagic flux in trametinib treated mice can elicit regression of established MIA-PaCa2 xenografts.

Trametinib plus chloroquine/hydroxychloroquine promote regression of RAS→RAF→MEK→ERK driven cancers.

To determine if the anti-neoplastic effects of combined trametinib plus autophagy inhibition with either chloroquine or ATG4B^{DN} observed *in vitro* or *in vivo* respectively might translate more broadly into additional tumor models, tumors generated by xenografting MIA-PaCa2 or BxPC3 cells into NOD/SCID mice were treated with vehicle control (control), trametinib, chloroquine or the combination of both trametinib plus chloroquine (Figs. 3e & f). Whereas chloroquine treatment had no effect on MIA-PaCa2 tumors, trametinib elicited a modest reduction in tumor growth (Fig. 3e). Similarly, single agent trametinib or chloroquine had only modest inhibitory effects on the growth of BxPC3 tumors. By contrast, the combination of trametinib plus chloroquine elicited striking regression of established Mia-PaCa2 or BxPC3 tumors (Figs. 3e & f). These observations were subjected to further scrutiny using mice xenografted with two *KRAS*-mutated PDA PDX models: PDX220 or PDX227, which were then treated as described above. In parallel, a cohort of PDX220 or PDX227 PDX-bearing mice were treated with a regimen of gemcitabine plus nab-paclitaxel that approximates the standard-of-care for a subset of human PDA patients (Figs. 3g & h) [25]. In this experiment, the combination of trametinib plus chloroquine/hydroxychloroquine not only resulted in tumor regression but was superior to gemcitabine plus nab-paclitaxel. Consistent with our treatment regimen, pERK1/2 was

decreased and the abundance of p62 increased in PDX227 tumors derived from mice treated with trametinib plus chloroquine (Ext. Fig. 3). To determine whether orthotopically engrafted tumors would respond to treatment, PDX220 fragments were implanted into the pancreata of NOD/SCID mice and treated 21 days later with vehicle control, trametinib, hydroxychloroquine or trametinib plus hydroxychloroquine. As observed previously, the growth of these tumors was substantially inhibited by the combination of trametinib plus chloroquine but not by either of the single agents (Ext. Figs. 4a-c). Moreover, mice treated with the combination of trametinib plus hydroxychloroquine demonstrated inhibition of [18F]-deoxyglucose (FDG) uptake as assessed by PET/CT imaging. By contrast, vehicle- or hydroxychloroquine-treated mice demonstrated continuous tumor growth and trametinib-treated mice demonstrated only a partial response.

Next, we tested whether the combination of trametinib plus chloroquine would promote regression of other tumor types driven either by mutationally activated *RAS* or *BRAF*. To that end, we employed PDX models of either *NRAS*-driven melanoma (HCI-Mel002 & NCI515677) or $BRAF^{V600E}$-driven colorectal cancer (HCI-CRC004). As before, PDX tumors were treated with vehicle control, trametinib, chloroquine or trametinib plus chloroquine (Figs. 3i-j & Ext. Fig. 5a). Under the conditions of this experiment, only the combination of trametinib plus chloroquine led to regression of all three PDX models. Importantly, mice treated with the combination therapy displayed no weight loss (Ext. Fig. 5b-e), however, side-effects of facial rash and hair loss were noted, although these were mitigated by reducing the dose of chloroquine to 25mg/kg, which remained effective in combination with trametinib (Ext. Fig. 5a). To further investigate the potential role of autophagy in the response of *RAS* mutated cancer cells to MEK1/2 inhibition we employed two $KRAS^{G12D}$/$TP53^{Null}$-driven mouse lung cancer cell lines (SC196 & SC274) derived from suitably manipulated $Kras^{FSF\text{-}G12D/+}$; $Trp53^{Frt/Frt}$; $Rosa^{FSF\text{-}CreERT2}$ mice [26]. Whereas MEK1/2 inhibition in SC274 cells led to increased autophagic flux, similar treatment of SC196 cells did not induce autophagic flux for reasons that are unclear (Ext. Figs. 6a, c, d). When assessed *in vitro*, we detected synergy between trametinib and chloroquine in SC274 cells but not in SC196 cells (Ext. Fig. 6b). Moreover, when tested in xenografted tumors in mice, only xenografted SC274 tumors displayed regression in response to the combination of trametinib plus chloroquine, whereas SC196 cell derived tumors failed to respond to this combination of agents (Ext. Figs. 6e-f). These data indicate that the ability of trametinib to promote autophagy in cultured $KRAS^{G12D}$/$TP53^{Null}$-driven lung cancer cell lines is predictive of their response, or lack thereof, to the combination of trametinib plus chloroquine in mice. Furthermore, these data are broadly consistent with the hypothesis that the *in vitro* and *in vivo* inhibitory effects of combined treatment with trametinib plus chloroquine is due to a tumor cell autonomous induction of protective autophagy by MEK1/2 inhibition that is abrogated by autophagy inhibitors such as chloroquine that convert an otherwise cytostatic response into a cytotoxic one. These data suggest that the combination of MEK1/2 inhibition plus chloroquine may promote regression of several tumor types in which RAS→RAF→MEK→ERK signaling is constitutively activated.

Partial response of a refractory pancreatic cancer patient to trametinib plus hydroxychloroquine.

We encountered a patient with metastatic pancreatic cancer in our GI malignancies clinic, who was refractory to all standard-of-care therapy options. The patient, a 68 year-old man, had been pre-treated with neo-adjuvant mFOLFIRINOX, adjuvant gemcitabine/capecitabine and with palliative gemcitabine/abraxane/cisplatin. The patient's best response was stable disease with the first two drug regimens and disease progression with the last. Moreover, the patient was displaying signs of PDA recurrence as evidenced by the development of celiac plexus pain and a rapid increase in the level of the PDA blood-borne cancer antigen 19–9 (CA19–9).

Given our compelling preclinical data, compassionate treatment of this patient was initiated on off-label, off-trial trametinib plus hydroxychloroquine (T/HCQ) starting at 2mg of trametinib and 400mg hydroxychloroquine daily in compliance with all relevant ethical regulations. Keeping the trametinib dose unchanged, the hydroxychloroquine was then escalated to 800mg daily and then to 600mg twice daily. After initiation of 2mg of trametinib plus 800mg of hydroxychloroquine the patient reported resolution of his celiac plexus pain. However, the patient's CA19–9 continued to rise from ~17,000 to ~33,000 during the first two weeks of treatment. However, once the patient began receiving 2mg of trametinib plus 1200mg of hydroxychloroquine daily, his CA19–9 levels declined precipitously by ~95% over the ensuing 2 months indicative of response (Fig. 4a). Moreover, CT imaging four months following initiation of T/HCQ therapy (2mg T/1200mg HCQ per day) indicated a 50% reduction in tumor burden by RECIST 1.1 criteria indicating a partial response (Figs. 4b-e). During the first 60 days that the patient received T/HCQ therapy, he experienced grade 1 rash and grade 1 fatigue. Moreover, since both trametinib and hydroxychloroquine have noted ocular and cardiac toxicities, we conducted monthly ophthalmologic exams and weekly electrocardiograms but without evidence of toxicity.

DISCUSSION

Results presented here are consistent with previous observations that autophagy serves as an adaptive and protective response to inhibition of RAS→RAF→MEK→ERK signaling in cancer [27–29]. Moreover, they are consistent with a companion manuscript that describes similar phenomena in PDA cells treated with ERK1/2 inhibitors (Bryant et al., *Nature Medicine*, Submitted). Similar observations have been reported in $BRAF^{V600E}$-driven melanoma, consistent with our analysis of *NRAS*-mutated melanoma PDX models (Fig. 3i, Ext. Fig. 5) [30]. Although we demonstrate a link between MEK1/2 inhibition and activation of the ULK1→AMPK→LKB1 axis leading to autophagy induction in PDA, it is likely other pathways are involved in autophagy induction in response to inhibition of RAS→RAF→MEK→ERK signaling.

Recently, it has been demonstrated that $ATG4B^{DN}$-mediated inhibition of autophagy promotes regression of $KRAS^{G12D}$/$TP53^{R172H}$-driven tumors in the KPC GEM model of PDA, but in a gene dosage dependent manner [24]. Whereas our data are consistent with these observations, our data also suggest that the dependence of pancreatic (and possibly other *RAS* mutated) cancer cells on autophagy becomes more acute in the face of pathway-

targeted inhibition of RAF→MEK→ERK signaling. Indeed, in our pre-clinical models, tumors were relatively resistant to single agent trametinib or chloroquine/hydroxychloroquine, but were exquisitely sensitive to the combination, unlike the situation with $BRAF^{V600E}$-driven brain tumors or melanoma which are initially sensitive to single agent $BRAF^{V600E}$ inhibition. Although previous work suggests that macroautophagy is dispensable for growth of *KRAS* mutated tumors and for the efficacy of chloroquine, even when used in combination with other agents, this work did not test the combination of MEK inhibitors plus chloroquine [31].

The status of *TP53* has been reported to determine whether autophagy inhibition can either inhibit or promote the progression of PDA in GEM models. In this case it was reported that PDA arising due to concomitant expression of $KRAS^{G12D}$ and silencing of TP53 in the pancreas was accelerated either by genetic ($ATG5^{Null}$ or $ATG7^{Null}$) or pharmacological (chloroquine) inhibition of autophagy [32]. By contrast, our data fail to support a role for TP53 in the response of PDA cells to combined inhibition of MEK1/2 plus autophagy. First, both MIA-PaCa2 cells ($TP53^{R248W}$) and the SC274 lung cancer cells ($TP53^{Null}$) are sensitive to combined inhibition of MEK1/2 plus autophagy. Furthermore, genetic analysis Patient 1, who responded to T/HCQ therapy, indicated mutational alteration of TP53 (data not shown). Hence, in our research, *TP53* status does not obviously diminish the anti-tumor effects of the T/HCQ combination (Ext. Figs. 6b, e-f).

It has previously been demonstrated that autophagic flux in cells of the pancreatic cancer microenvironment (e.g. stellate cells or macrophages) can contribute to tumor maintenance [24, 33]. Here, using tumor cell specific expression of $ATG4B^{DN}$ in MIA-PaCa2 cells, we demonstrate a tumor cell autonomous role for autophagy to protect cells from MEK1/2 inhibition. Although the anti-tumor effects of this regimen may be further enhanced by systemic inhibition of autophagy within the tumor microenvironment, combined pharmacological blockade of MEK1/2 and autophagy in the malignant cell appears sufficient for tumor regression[34]. Moreover, there are newer and more specific inhibitors of autophagy that target the VPS34 class III PI3'-kinase or the ULK1/ATG1 protein kinase that may warrant testing in combination with inhibitors of RAS→RAF→MEK→ERK signaling [10, 35, 36].

Finally, since both trametinib and hydroxychloroquine are orally administered, FDA-approved drugs [37–39], these observations were translated to the clinic for a single, heavily pre-treated PDA patient. Remarkably, the T/HCQ combination resulted in substantial reduction in this patient's overall tumor burden, CA19–9 tumor marker, and resolution of debilitating cancer pain. Moreover, the safety and tolerability of the T/HCQ combination is likely to be superior to traditional cytotoxic chemotherapy for PDA patients. However, caution must be exercised in interpreting and extrapolating from the response of a single patient such that we urge that the potential benefits of T/HCQ therapy be tested in PDA patients only in the context of suitably designed clinical trials. However, the combination of compelling preclinical data and the striking response of the first patient to be treated with the T/HCQ combination provides a compelling impetus to conduct a rigorous clinical trial to test T/HCQ therapy on overall response rate and measures of survival in PDA patients. Furthermore our pre-clinical data suggests that the testing of this combination of agents may

eventually be warranted in patients with other malignancies driven by mutationally activated *RAS/BRAF* genes such as melanoma, colon or lung cancer.

METHODS

Cells Lines.

MiaPaCa2 and BxPC3 cell lines were originally obtained from ATCC and maintained in 1:1 DMEM/F-12 (Gibco) with 10% fetal bovine serum (FBS). The PDX220 cell line was derived from a pancreatic cancer patient derived xenograft by mechanical dissociation of tumor tissue followed by culture in 1:1 DMEM/F-12 (Gibco) with 10% FBS. SC196 and SC274 cell lines were derived from tumors initiated by intra-tracheal infection of $Kras^{FSF\text{-}G12D/+}; p53^{Frt/Frt}; Rosa^{FSF\text{-}CreERT2}$ mice with an adenoviral vector expressing FLP recombinase. Cell lines were established from lungs harvested from mice 6–12 weeks after tumor initiation by enzymatic and mechanical dissociation. Cell lines were periodically tested for mycoplasma contamination and discarded if positive.

Autophagic Flux Assay.

pBabePuro: mCherry-GFP-LC3 was obtained from Addgene (a gift from Jayanta Debnath; plasmid # 22418) and the mCherry-GFP-LC3 cDNA was introduced into the lentiviral construct pUltra-Hot resulting in pUltra-Auto. Lentivirus derived from pUltra-Auto was transduced into cell lines resulting in AFR cell lines. AFR cell lines were subjected to various treatments, trypsinized and then resuspended for analysis of of GFP and mCherry fluorescence by flow cytometry using a BD FACS-Canto II. Cells were co-stained with DAPI at 1ug/ml to exclude dead cells. mCherry/GFP ratio was generated using FACSDIVA v8.0.1 software and gates were set for low/intermediate/high populations and maintained throughout the experiment. All experiments were conducted in triplicate and significance of difference in autophagic flux was calculated using a two-tailed t-test.

Lentiviral Transduction.

pUltra-Auto and TetR-Flag-ATG4B DN (a gift from Andrew Thorburn) lentiviral constructs were used to express mCherry-GFP-LC3 and ATG4B DN respectively in cell lines. To general lentivirus 3×10^6 HEK293T cells per 10cm dish in 6 mL of 1:1 DMEM/F12 with 10%(v/v) FBS were plated 6 hours prior to transfection. Transfection of vector DNA (3μg), psPAX2 (3μg), and CMV-VSVG (1.5μg) were combined in 600μL of sterile PBS and 18μL of FugeneHD (Promega) was added to the mixture per 10 cm dish. The transfection mixture was incubated for 15 minutes at room temperature then added dropwise to the HEK293T cells. Media was exchanged for fresh 1:1 DMEM/F12 with 10% FBS the next day. After 48 hours, supernatants were harvested and filtered through 0.45uM filters, which were then added fresh to target cell lines or flash frozen for storage in liquid nitrogen for later use. When performing lentiviral transduction 8μg/mL of polybrene was added. After 6 hours viral transduction media was exchanged for fresh media. After 48 hours cells were selected via FACS for mCherry/GFP expression or puromycin at 10μg/mL for pUltra-Auto orTetR-Flag-ATG4B^{DN} transduction respectively.

AMPK and ULK1 Dominant Negative Expression.

Mia-PaCa2^{AFR} were transiently transfected with pcDNA3 (Vector), or vectors encoding AMPKα (WT or K45R, gift from Morris Birnbaum; Addgene plasmids #15991 and 15992) or myc-mULK1 (WT or M92A, gift from Do-Hyung Kim; Addgene plasmids # 31961 and # 31962) utilizing Lipofectamine 3000 (Invitrogen). For confirmation of expression, cells lysates were harvested 48 hours after transfection for analysis by immunoblotting. To test effects on autophagic flux, AFR cells transiently transfected with the various plasmid constructs were treated with trametinib beginning 24 hours after transfection and analyzed by flow sytomrtery 48 hours following trametinib addition.

Immunoblotting.

Cells were washed three times with ice cold PBS, detached by adding ice cold PBS with 5mM EDTA, pelleted by centrifugation at 250xg for 5 minutes, and then solubilized using RIPA buffer containing phosphatase and protease inhibitors (Thermo) at 4^{o}C for one hour. Detergent insoluble material was removed by centrifugation at 15,000xg for 10 minutes at 4^{o}C. Protein concentrations were determined by BCA Protein Assay (Thermo). Membranes were blocked in Odyssey Blocking Buffer (LI-COR) for 1 hour then immunoblotted with the following primary antibodies overnight in Odyssey Blocking Buffer: phospho-ERK 1:1000 T202/Y204 (CST D13.14.4E), total ERK1/2 1:1000 (CST), p62 1:500 (Progen p62-C), LC3A/B 1:500 (CST), phospho-LKB1 S428 1:500 (Abcam Ab63473), LKB1 1:500 (CST D60C5), phospho-AMPK T172 1:500 (CST 40H9), AMPK 1:500 (CST D5A2), phospho-ULK1 S555 1:500 (CST D1H4), ULK1 1:500 (CST D8H5), and ATG4B 1:500 (CST D162R). Standard immunoblotting procedures were then followed with Alexa 680 and 800 conjugated species specific secondary antibodies. Immunoblotting was visualized with a LI-COR CLx infrared scanner.

In Vitro Synergy Assay.

To evaluate synergy *in vitro*, cells were seeded into 384-well plates in complete medium, cultured overnight, and then treated in quadruplicate with trametinib or chloroquine, either alone or in various combinations in 20%(v/v) medium in EBSS. At end-point, medium was removed and cells were assayed using ATPlite 1step (Perkin Elmer) according to the manufacturer's protocol. Luminescence was quantified using a Perkin Elmer Envision plate reader, normalized to control, and analyzed with Combenefit software (Loewe model) [40].

In Vitro Incuycte Caspase 3/7 and cell death assays.

Cell lines were seeded at 4,000–10,000 cells/well in the wells of a 96-well plate (100μL RPMI/10% FBS/1% Pen/Strep per well). After 24 hours, cells were treated with DMSO control, trametinib, chloroquine, or trametinib plus chloroquine in at least triplicate. To detect apoptosis, 5nM Incucyte Caspase-3/7 Green Apoptosis Assay Reagent (Essen Bioscience, Cat#: 4440) was added to each well. To detect cell death, 250nM Incucyte Cytotox Red Reagent (Essen Bioscience, Cat#: 4632) was added to each well. Cells were imaged every 2 hours using the IncuCyte live cell anlysis system for 48 hours with data collection by the Incucyte ZOOM 2016B accompanying software. GFP-positive (Caspase 3/7 positive cells) or RFP-positive (dead cells) and total confluence was recorded at each

time point. One-way ANOVA was used to determine statistical significance and significance for each treatment was compared to DMSO control.

Mice.

NOD/SCID mice were bred and maintained in a pathogen-free facility by the Pre-clinical Research Resource (PRR) at the Huntsman Cancer Institute. All animal experiments were performed in accordance with protocols approved by the University of Utah Institutional Animal Care and Use Committees and we have complied with all relevant ethical regulations.

Xenograft Assays.

Xenografted tumors were established by sub-cutaneous injection of 2×10^6 MIA-PaCa2 or BxPC3 cells resuspended in 100μL of Matrigel into NOD/SCID mice and allowed to establish. Treatment was then initiated with vehicle control (corn oil), trametinib at 1mg/kg, chloroquine at 25–50mg/kg or the combination of trametinib plus chloroquine at the aforementioned dosages via oral gavage daily. In the case of Mia-PaCa2 cells expressing the TetR-Flag-ATG4B^{DN} construct, mice were treated with vehicle control (corn oil), trametinib at 1mg/kg via oral gavage daily and either standard chow or doxycycline chow (625mg/kg). Tumors were measured twice weekly via calipers and tumor volume was calculated by volume = $4/3*\pi*(\text{length+width})/2)/2)^3$. Significance of difference in tumor size was calculated by a two-tailed t-test.

Patient Derived Xenograft Assays.

Tumor tissue was obtained from patients who provided written informed consent according to a tissue collection protocol (University of Utah IRB 89989 and 10924) approved by the Huntsman Cancer Institute Institutional Review Board and subcutaneously implanted into NOD/SCID mice for generation of PDA PDX and into NSG mice for the generation of melanoma or colorectal PDX. PDX220 was derived from a neck metastasis from a 53 year old woman who had received prior treatment with FOLFIRINOX, Gem/Abraxane, FOLFOX, and 5-FU/Cisplatin with *KRAS*^{G12V}, *MTOR*$^{A1828\_A1831del}$, *TP53*^{V173G}, *ARID1A*^{Q1330*}, *CDKNA2A*$^{p16INK4a\ Q50*,}$ and *TGFBR2*^{R537C} mutations. PDX227 was derived from a 75 year old man from a primary resection sample that had squamous differentiation prior to any treatment with a *BRCA2*^{S1982Rfs*22} mutation. HCI-Mel002 was derived from a cutaneous biopsy of an *NRAS*-mutated (NRAS^{Q61R}) melanoma isolated from a previously untreated 85 year old woman. HCI-CRC004 was derived from a resection specimen of a *BRAF*-mutated (BRAF^{V600E}) colorectal cancer from a previously untreated 63 year old woman. NCI 516677 (515677–202-R, Passage 3) was obtained from the public NCI PDX bank and information regarding patient demographics, site, prior treatment and genotype are publically available. These tumors were propagated and expanded. Upon experiment initiation 50–70mg tumor fragments were implanted bilaterally into the flanks of NOD/SCID mice (PDA PDX) or NSG mice (melanoma and colorectal PDX). When established tumors were measurable, treatment was initiated with vehicle control (corn oil), trametinib (1mg/kg), chloroquine (25–50mg/kg), hydroxychloroquine (40mg/kg) or the combination of trametinib and chloroquine/hydroxychloroquine at the aforementioned single agent dosages via oral gavage. For gemcitabine/nab-paclitaxel treatment, 100mg/kg of

gemcitabine and 10mg/kg of nab-paclitaxel was infused via tail vein weekly for three weeks with one week off approximating the dosing schedule for pancreatic cancer patients. Tumors were measured and tumor volumes calculated as previously described.

Preclinical Imaging,

Mice were anesthestized with 1.5–2% sevoflurane prior to injecting approximately 0.5mCi of [^{18}F]-fluorodeoxyglucose (FDG). CT imaging was performed using a NanoScan™ SPECT/CT scanner followed by PET and MRI imaging using a NanoScan™ PET/MRI scanner (Mediso Medical Imaging, Budapest). The animal remained anesthetized and immoblized in a common MultiCell™ animal chamber to provide intrinsic spatial co-registration of CT, MRI, and PET images. T1-weighted Gradient Echo (GRE) images and T2-weighted 2D Fast Spin Echo (FSE) images were acquired prior to initiating a 20-minute PET emission scan at 60 minutes post-injection of FDG. Quantitative analysis was performed using VivoQuant (inviCRO, Boston, MA). Metabolic Tumor Volumes (MTV) were defined semi-automatically using a minimum threshold of the Standardized Uptake Value (SUV). Total Lesion Glycolysis (TLG) was then calculated as the MTV x SUV mean. For each mouse, the optimal SUV threshold was defined on the baseline images and applied consistently to the post-treatment images. Changes in TLG following treatment was then calculated for each mouse relative to the pre-treatment baseline TLG.

Immunohistochemistry.

Tumor-bearing mice were euthanized and tumor tissues were harvested and fixed in 10% (v/v) formalin overnight. Tissues were transferred to 70%(v/v) ethanol, embedded in paraffin, and four-micron sections were cut. Immunohistochemistry (IHC) was performed manually on Sequenza slide staining racks (Thermo). Sections were treated with Bloxall (Vector labs) followed by horse serum (Vector labs), primary antibody for phospho-ERK (CST D13.14.4E) 1:600, p62 (Progen GP62-C) 1:200 and ATG4B 1:200 (CST D162R), then anti-Guinea Pig (Vectastain) or anti-Rabbit (Vector Labs) HRP-polymer. The slides were developed with DAB (Vector) and counterstained with hematoxylin.

Statistical Testing:

Two-sided t-testing was used for all autophagy flux reporter assays comparing control high (red) versus experimental high autophagic flux data. Two-sided t-testing was also used for all in vivo tumor growth assay data compared at the days noted in the graphs. One-way ANOVA testing was used to compare groups for all Incucyte experiments.

DATA AVAILABILITY STATEMENT

The data that support the findings of this study are available from the corresponding author upon reasonable request.

Extended Data

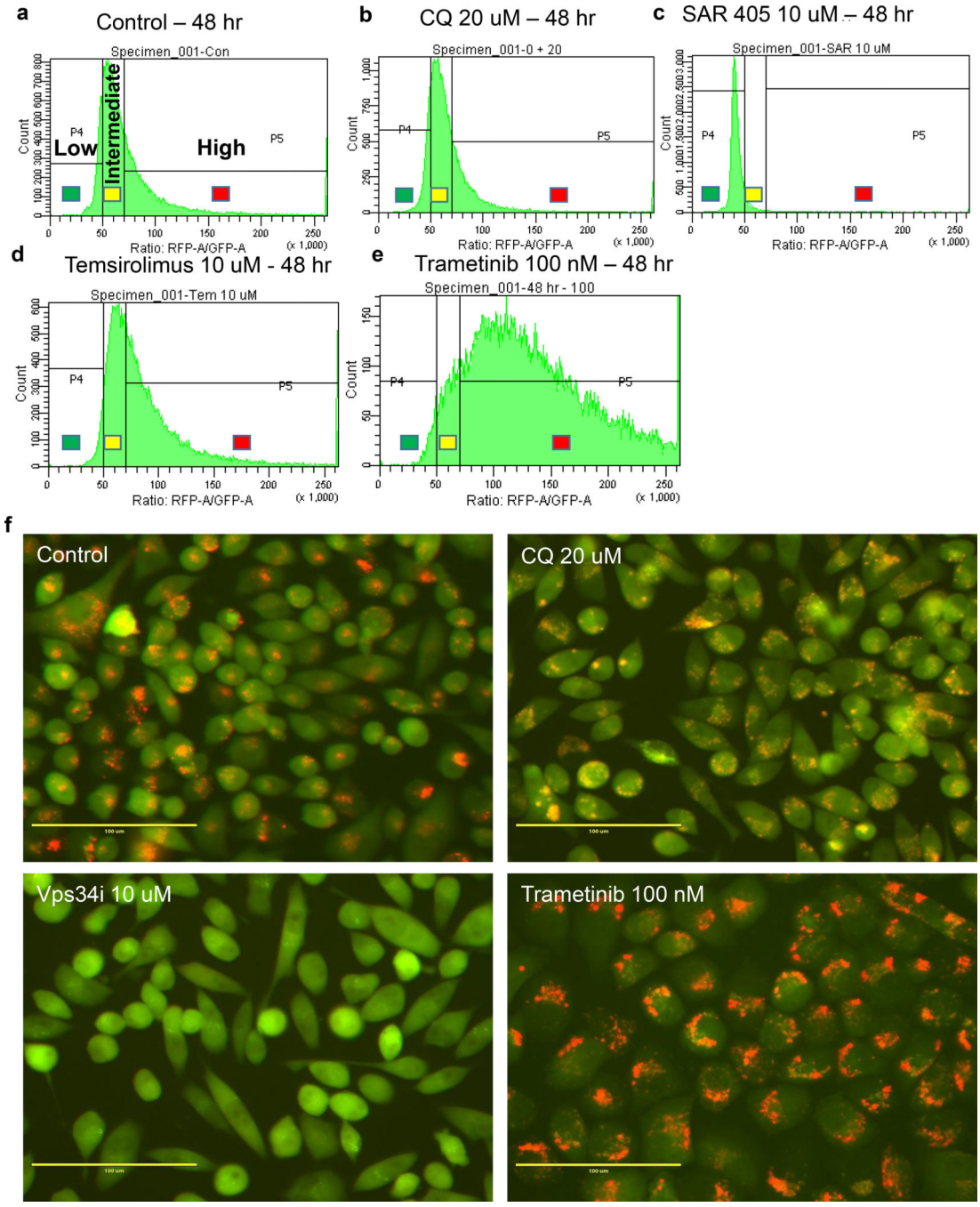

Ext. Figure 1. Flow cytometry analysis of autophagic flux reporter with autophagy inhibitors and inducers.

a-e: Autophagic flux was assessed by flow cytometry in Mia-PaCa2^{AFR} cells following 48 hours treatment with control, chloroquine (CQ), SAR-405, temsirolimus, or trametinib. Experiments were repeated three times with similar results.

f: Autophagic flux was assessed by fluorescent imaging in Mia-PaCa2^{AFR} cells following 48 hours treatment with control, chloroquine (CQ), VPS34i (SAR-405), or trametinib. Experiments were repeated three times with similar results.

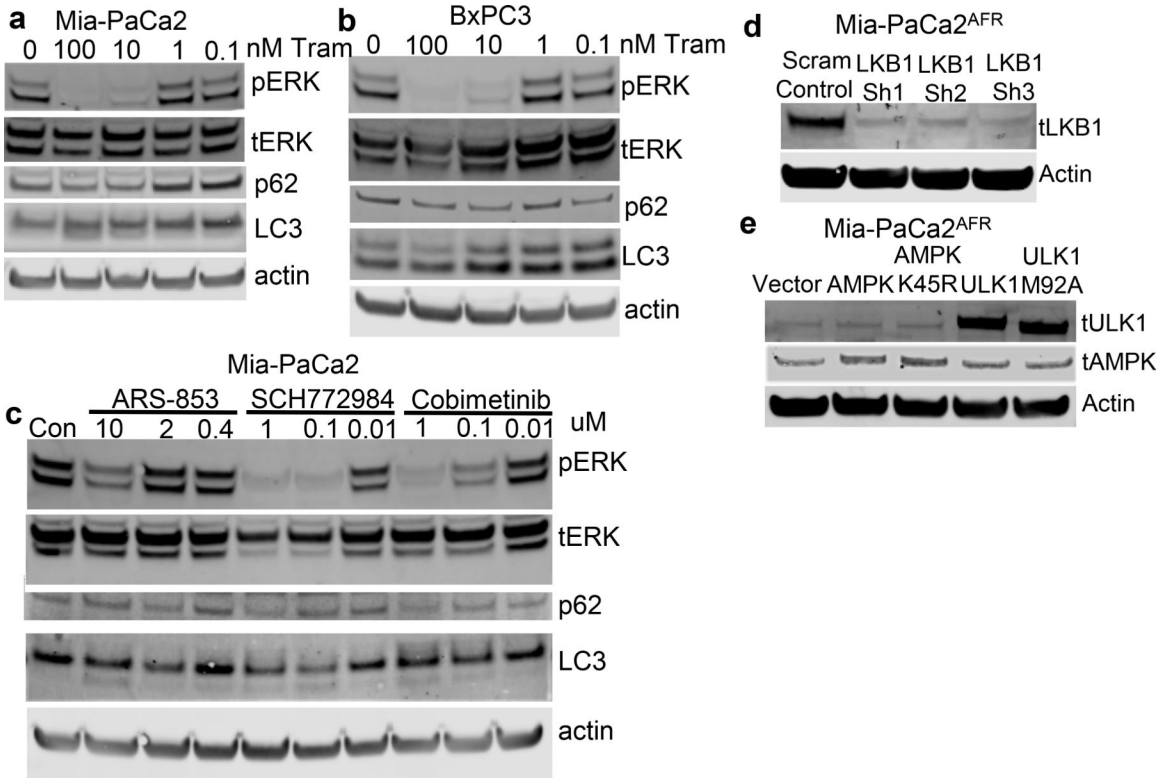

Ext. Figure 2. Inhibition of RAS→RAF→MEK→ERK signaling pathway induces autophagic flux (AF) as seen by p62 degradation and LC3 conversion in pancreatic cancer cells.

a & b: Cell lysates prepared from Mia-PaCa2 (a) or BxPC3 (b) cells treated with 0.1–100 nM of trametinib for 48 hours were analyzed by immunoblotting for the phosphorylation (p) or total (t) abundance of ERK1/2, p62, LC3, or actin as indicated. Experiments were repeated three times with similar results.

c: Cell lysates prepared from Mia-PaCa2 cells treated with ARS-853 (KRAS^{G12C}i), SCH772984 (ERKi), or cobimetinib (MEKi) for 48 hours were analyzed by immunoblotting for the phosphorylation (p) or total (t) abundance of ERK1/2, p62, LC3, or actin as indicated. Experiments were repeated three times with similar results.

d: Cell lysates prepared from Mia-PaCa2^{AFR} cells transiently expressing exogenous ULK1 WT, ULK^{M92A} (dominant negative), AMPK WT, or AMPK^{K45R} (dominant negative) were analyzed by immunoblotting for ULK1, AMPK, or actin as indicated. Experiments were repeated three times with similar results.

e: Cell lysates prepared from Mia-PaCa2^{AFR} cells lentivirally transduced with shRNAs targeting LKB1 or scrambled control were analyzed by immunoblotting for LKB1 or actin as indicated. Experiments were repeated three times with similar results.

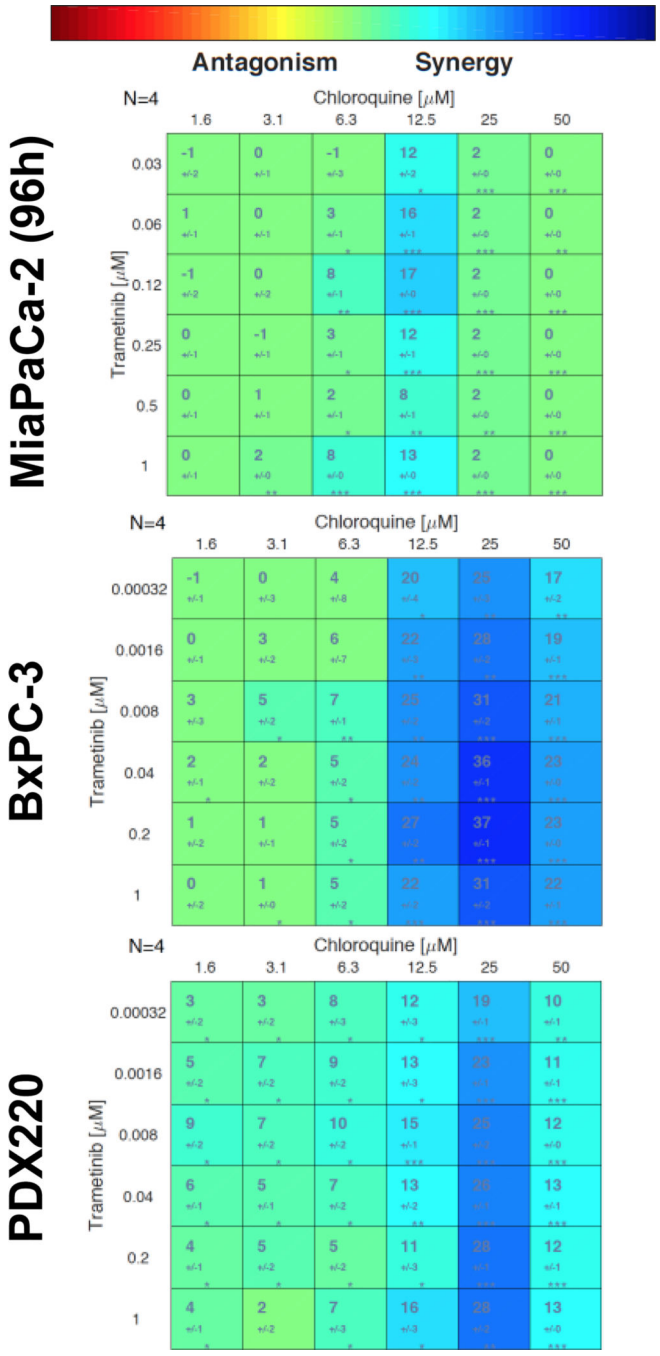

Ext. Figure 3. Trametinib and chloroquine are synergistically cytotoxic in vitro.

Mia-PaCa2 cells, BxPC3 and PDX220 cells were treated for 48–96 as indicated with trametinib and chloroquine and analyzed for cell viability by ATPlite assay. Synergy scores were generated utilizing Combenefit Software. Experiments were repeated four times with similar results.

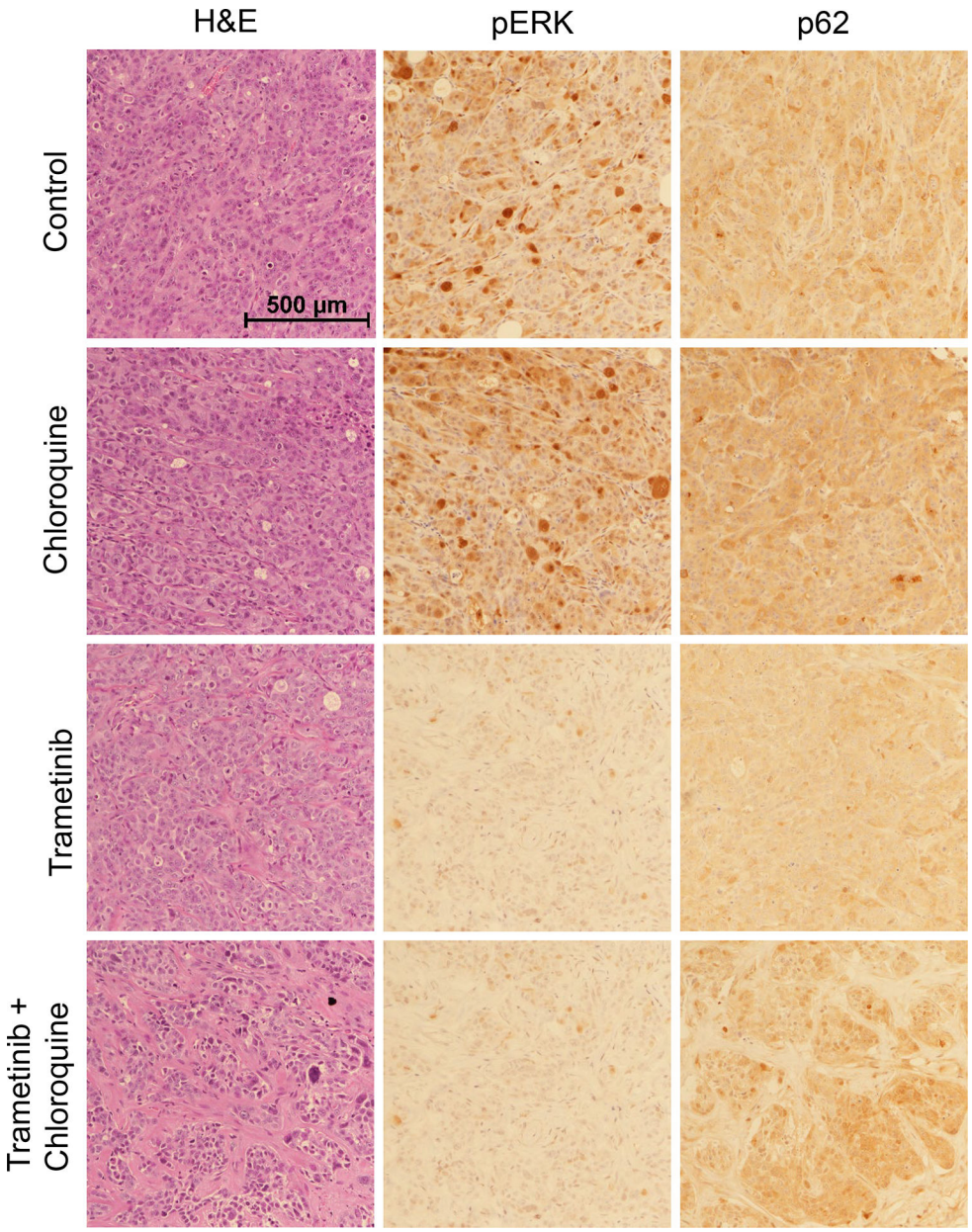

Ext. Figure 4. Treatment of pancreatic tumors with trametinib and chloroquine results in decreased pERK and increased p62 abundance respectively.

Representative images of immunohistochemical analysis of sections of PDX 227 tumors that were treated with 1. vehicle (Control), 2. trametinib; 3. chloroquine or; 4. the combination of both agents. Sections were stained with H&E or with antisera against pERK1/2 or p62 as indicated. Experiments were repeated four times with similar results. Scale bar is 500 μM located in the bottom right of the upper left panel and is consistent for all images.

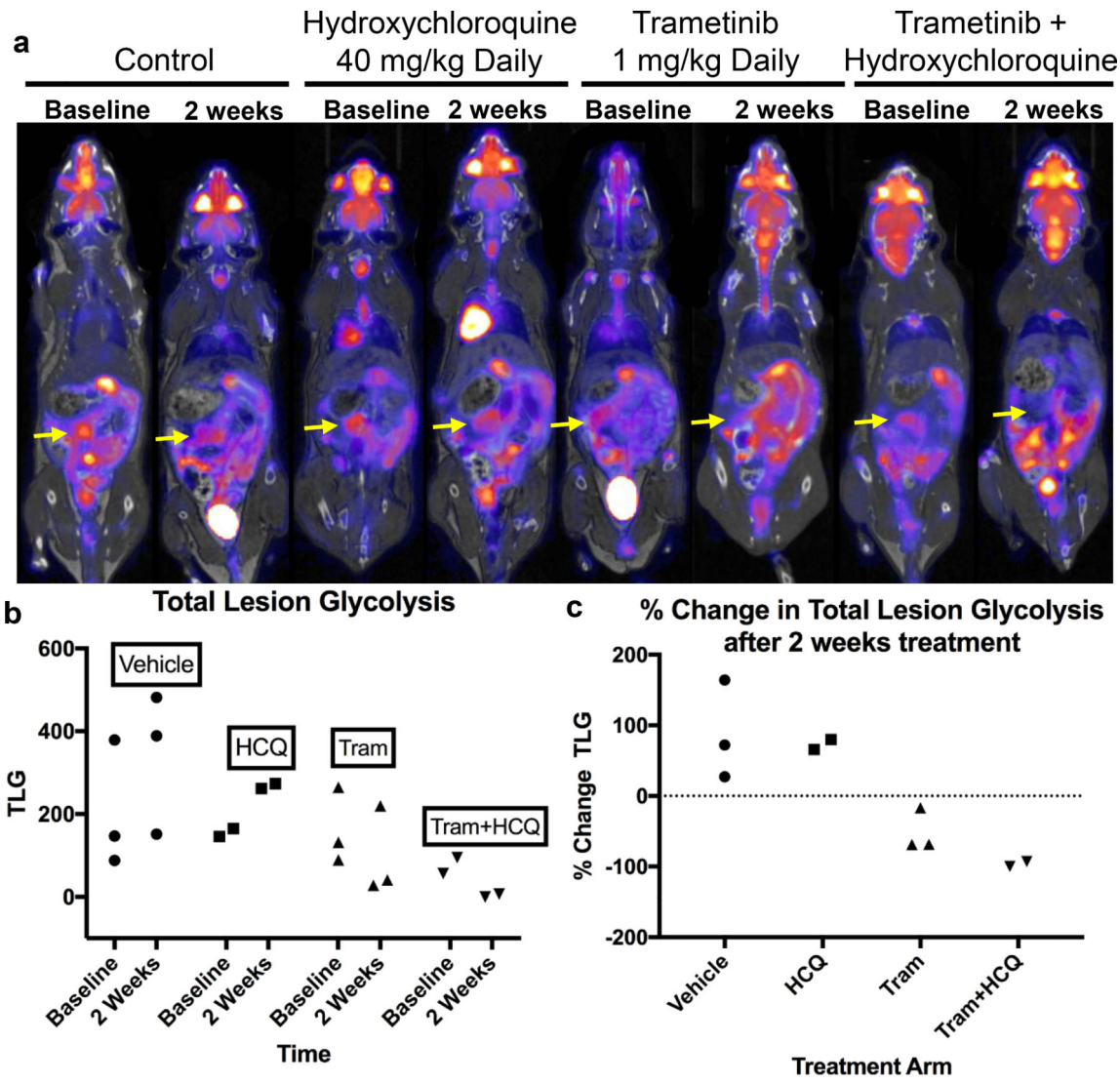

Ext. Figure 5. Treatment of orthopically xenografted pancreatic tumors with trametinib and hydroxychloroquine demonstrates regression consistent with subcutaneous xenografts.

a: PDX220 tumors were orthotopically transplanted and after 3 weeks were imaged via FDG-PET/CT for baseline. They were then treated with trametinib, hydroxychloroquine or trametinib plus hydroxychloroquine for 2 weeks prior to re-imaging. n=3 for control; n=2 for HCQ; n=3 for trametinib; n=2 for trametinib+hydroxychloroquine.

b & c: Quantification of total lesion glycolysis (b) and % change (c) for individual tumors within each treatment group.

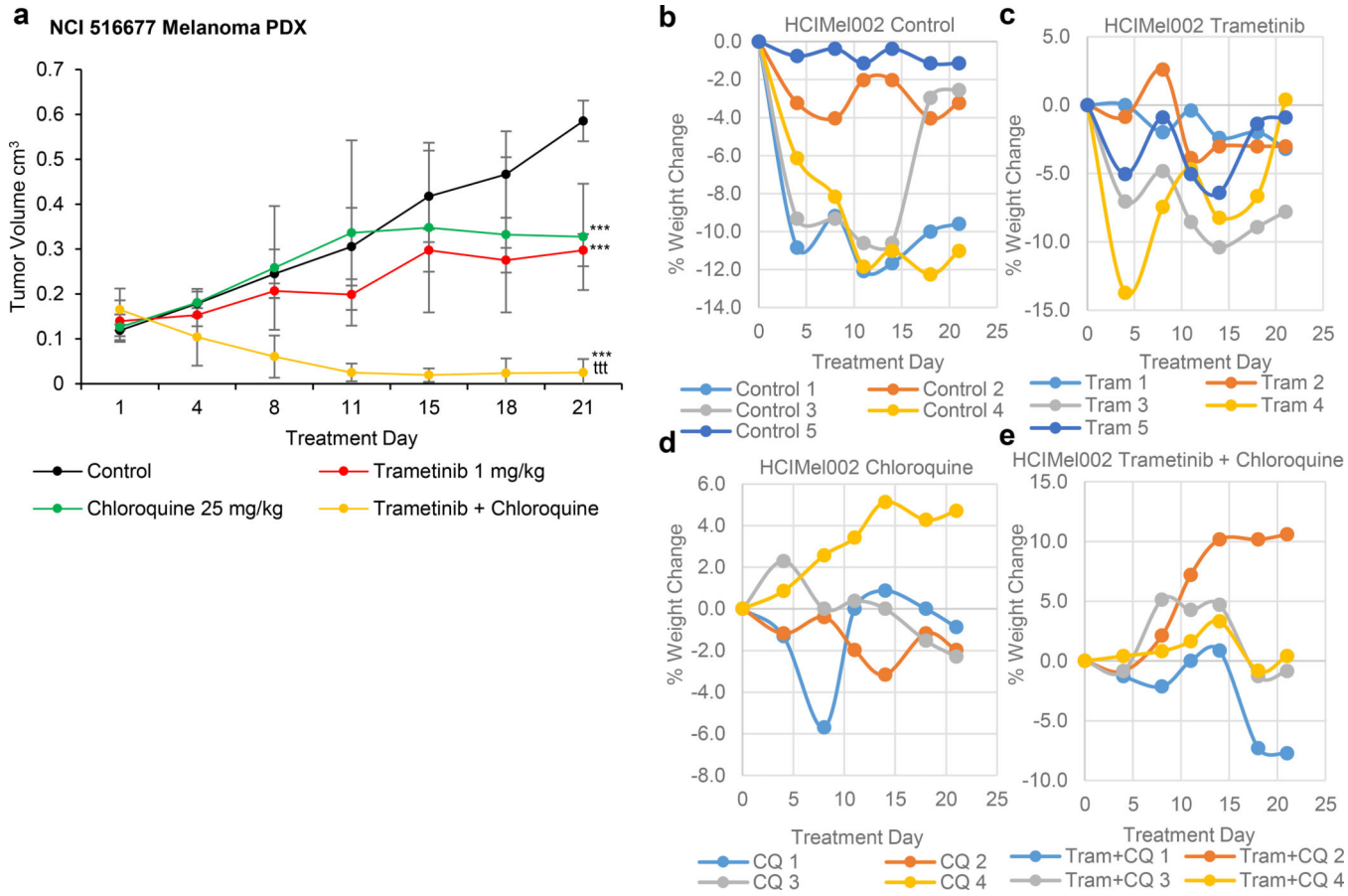

Ext. Figure 6. Regression of established NRAS driven melanoma tumors by combined inhibition of MEK1/2 plus chloroquine.

a. The growth of *NRAS*-mutated melanoma (NCI515677) PDX was assessed over 21 days in mice treated with: 1. vehicle (Control), 2. trametinib (1mg/kg), 3. chloroquine (25mg/kg) or; 4. the combination of both agents at the aforementioned doses as indicated. n=4 for all treatment groups except combination of both agents n=5. Center values are the mean; statistical testing was performed by two-sided t-test; ***p<0.001 vs. control; ^{ttt}p<0.001 vs. trametinib. Error bars represent SD.

b-e. The percentage weight change of HCI-Mel002 *NRAS*-mutated PDX was assessed over 21 days in mice treated with: b. vehicle (Control), c. trametinib (1mg/kg), d. chloroquine (50mg/kg) or; e. the combination of both agents at the aforementioned doses as indicated. However, side-effects of facial rash and hair loss were noted.

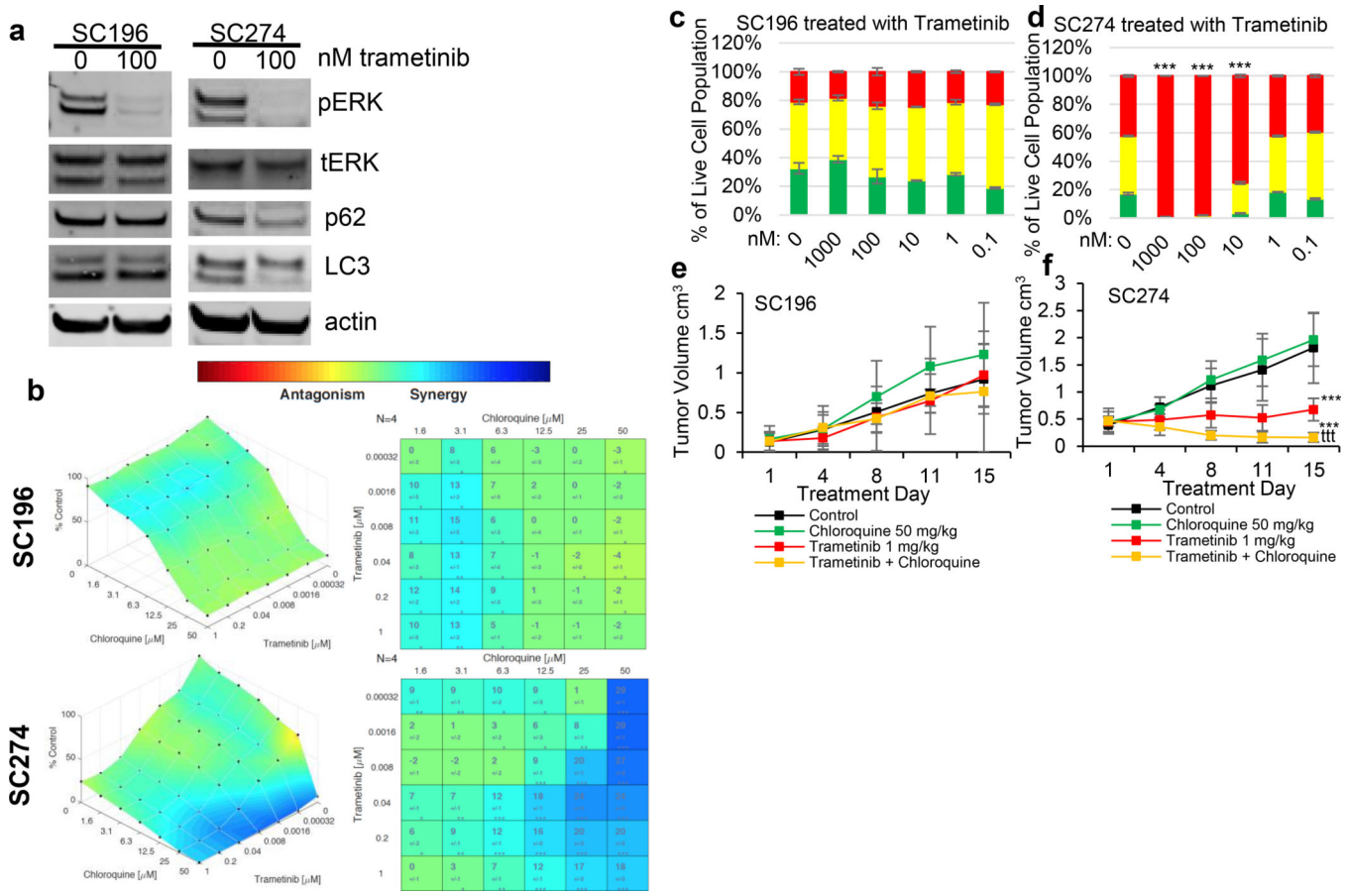

Ext. Figure 7. Lack of autophagy induction by MEK1/2 inhibition results in resistance to combined trametinib and chloroquine treatment.

a: Cell lysates prepared from two suitably manipulated $KRAS^{G12D}/TP53^{Null}$ mouse lung cancer-derived cell lines, SC196 or SC274 treated with 100nM of trametinib were analyzed by immunoblotting for the phosphorylation (p) or total (t) abundance of ERK1/2, p62, LC3, or actin as indicated. Experiments were repeated three times with similar results.

b: SC196 and SC274 $KRAS^{G12D}/TP53^{Null}$ mouse lung cancer cells were treated for 48 hours respectively with trametinib and chloroquine and analyzed for cell viability by ATPlite assay. Synergy scores were generated utilizing Combenefit Software. Experiments were repeated four times with similar results.

c & d: Autophagic flux was measured in $SC196^{AFR}$ (c) or $SC274^{AFR}$ (d) following treatment with 0.1–1000nM trametinib for 48 hours.. n=3; center values are the mean; statistical testing was performed by two-sided t-test of control high (red) versus experimental high; ***p<0.001 vs. control. Error bars represent SD.

e & f: The growth of SC196 (e) or SC274 (f) $KRAS^{G12D}/TP53^{Null}$ mouse lung cancer derived tumors in xenografted mice treated with: 1. vehicle (Control), 2. trametinib (1mg/kg), 3. chloroquine (50mg/kg) or; 4. the combination of both agents was assessed over ~15 days as indicated. n=10 for all treatment groups.. Center values are the mean; statistical testing was performed by two-sided t-test;***p<0.001 vs. control; ^{ttt}p<0.001 vs. trametinib. Error bars represent SD.

Supplementary Material

Refer to Web version on PubMed Central for supplementary material.

ACKNOWLEDGEMENTS

We thank the members of the McMahon Lab for their support, advice, guidance, comments and discussions during the course of this work. Additionally we thank Ignacio Garrido-Laguna (HCI/Univ. of Utah), Margaret Tempero, Eric Collisson & Frank McCormick (U.C. San Francisco), Eileen White (Rutgers University), David Tuveson (Cold Spring Harbor), and Kenneth Olive (Columbia) for advice and guidance, Jean Mulcahy-Levy & Andrew Thorburn (U.C. Denver) for inspiration, advice, guidance and reagents, Hartmut Land (University of Rochester Medical Center) and Kevan Shokat (UCSF) for providing reagents, NCI Patient-Derived Models Repository for supplying the NCI-516677 *NRAS*-mutated melanoma PDX, Katie Owings, David Lum and the HCI Preclinical Research Resource for assistance with tumor xenografts and drug treatments and Mark Silvis for assistance with drug dosing. CK & MM wish to acknowledge the collegiality of Kirsten Bryant and Channing Der (University of North Carolina, Chapel Hill) for ongoing discussions and for sharing data in advance of publication.

M.M. acknowledges financial support from the National Cancer Institute (R01-CA176839, R01-CA131261 & P30-CA042014), the Pancreatic Cancer Collective, Melanoma Research Alliance and the Huntsman Cancer Foundation. E.L.S. was supported in part by a Career Award for Medical Scientists from the Burroughs Wellcome Fund, a V Scholar Award, the Huntsman Cancer Foundation, and the NIH (R01CA212415). B.E.W. acknowledges support from the National Cancer Institute and DoD (U54CA224076 and W81XWH1410417). A.L.W. acknowledges support from the Huntsman Cancer Foundation. C.G.K acknowledges support from the Huntsman Cancer Foundation. A.M.B. acknowledges support from Fondation pour la Recherché Medicale (FDM20150633361) and Societe Francaise de Dermatologie.

LITERATURE CITED

1. Siegel RL, Miller KD, and Jemal A, Cancer Statistics, 2017. CA Cancer J Clin, 2017 67(1): p. 7–30. [PubMed: 28055103]
2. Li D, et al., Pancreatic cancer. Lancet, 2004 363(9414): p. 1049–57. [PubMed: 15051286]
3. Gao J, et al., Integrative analysis of complex cancer genomics and clinical profiles using the cBioPortal. Sci Signal, 2013 6(269): p. pl1. [PubMed: 23550210]
4. Cerami E, et al., The cBio cancer genomics portal: an open platform for exploring multidimensional cancer genomics data. Cancer Discov, 2012 2(5): p. 401–4. [PubMed: 22588877]
5. Collisson EA, et al., A central role for RAF-->MEK-->ERK signaling in the genesis of pancreatic ductal adenocarcinoma. Cancer Discov, 2012 2(8): p. 685–93. [PubMed: 22628411]
6. Infante JR, et al., A randomised, double-blind, placebo-controlled trial of trametinib, an oral MEK inhibitor, in combination with gemcitabine for patients with untreated metastatic adenocarcinoma of the pancreas. Eur J Cancer, 2014 50(12): p. 2072–81. [PubMed: 24915778]
7. Kimura S, Noda T, and Yoshimori T, Dissection of the autophagosome maturation process by a novel reporter protein, tandem fluorescent-tagged LC3. Autophagy, 2007 3(5): p. 452–60. [PubMed: 17534139]
8. Gump JM and Thorburn A, Sorting cells for basal and induced autophagic flux by quantitative ratiometric flow cytometry. Autophagy, 2014 10(7): p. 1327–34. [PubMed: 24915460]
9. Klionsky DJ, et al., Guidelines for the use and interpretation of assays for monitoring autophagy (3rd edition). Autophagy, 2016 12(1): p. 1–222. [PubMed: 26799652]
10. Ronan B, et al., A highly potent and selective Vps34 inhibitor alters vesicle trafficking and autophagy. Nat Chem Biol, 2014 10(12): p. 1013–9. [PubMed: 25326666]
11. Patricelli MP, et al., Selective Inhibition of Oncogenic KRAS Output with Small Molecules Targeting the Inactive State. Cancer Discov, 2016 6(3): p. 316–29. [PubMed: 26739882]
12. Gilmartin AG, et al., GSK1120212 (JTP-74057) is an inhibitor of MEK activity and activation with favorable pharmacokinetic properties for sustained in vivo pathway inhibition. Clin Cancer Res, 2011 17(5): p. 989–1000. [PubMed: 21245089]

13. Rice KD, et al., Novel Carboxamide-Based Allosteric MEK Inhibitors: Discovery and Optimization Efforts toward XL518 (GDC-0973). ACS Med Chem Lett, 2012 3(5): p. 416–21. [PubMed: 24900486]
14. Morris EJ, et al., Discovery of a novel ERK inhibitor with activity in models of acquired resistance to BRAF and MEK inhibitors. Cancer Discov, 2013 3(7): p. 742–50. [PubMed: 23614898]
15. Lito P, et al., Allele-specific inhibitors inactivate mutant KRAS G12C by a trapping mechanism. Science, 2016 351(6273): p. 604–8. [PubMed: 26841430]
16. Zheng B, et al., Oncogenic B-RAF negatively regulates the tumor suppressor LKB1 to promote melanoma cell proliferation. Mol Cell, 2009 33(2): p. 237–47. [PubMed: 19187764]
17. Kim J, et al., AMPK and mTOR regulate autophagy through direct phosphorylation of Ulk1. Nat Cell Biol, 2011 13(2): p. 132–41. [PubMed: 21258367]
18. Egan DF, et al., Phosphorylation of ULK1 (hATG1) by AMP-activated protein kinase connects energy sensing to mitophagy. Science, 2011 331(6016): p. 456–61. [PubMed: 21205641]
19. Mihaylova MM and Shaw RJ, The AMPK signalling pathway coordinates cell growth, autophagy and metabolism. Nat Cell Biol, 2011 13(9): p. 1016–23. [PubMed: 21892142]
20. Chou TC, Drug combination studies and their synergy quantification using the Chou-Talalay method. Cancer Res, 2010 70(2): p. 440–6. [PubMed: 20068163]
21. Vessoni AT, et al., Chloroquine-induced glioma cells death is associated with mitochondrial membrane potential loss, but not oxidative stress. Free Radic Biol Med, 2016 90: p. 91–100. [PubMed: 26577174]
22. Boya P, et al., Mitochondrial membrane permeabilization is a critical step of lysosome-initiated apoptosis induced by hydroxychloroquine. Oncogene, 2003 22(25): p. 3927–36. [PubMed: 12813466]
23. Fujita N, et al., An Atg4B mutant hampers the lipidation of LC3 paralogues and causes defects in autophagosome closure. Mol Biol Cell, 2008 19(11): p. 4651–9. [PubMed: 18768752]
24. Yang A, et al., Autophagy Sustains Pancreatic Cancer Growth through Both Cell-Autonomous and Nonautonomous Mechanisms. Cancer Discov, 2018 8(3): p. 276–287. [PubMed: 29317452]
25. Awasthi N, et al., Comparative benefits of Nab-paclitaxel over gemcitabine or polysorbate-based docetaxel in experimental pancreatic cancer. Carcinogenesis, 2013 34(10): p. 2361–9. [PubMed: 23803690]
26. Young NP, Crowley D, and Jacks T, Uncoupling cancer mutations reveals critical timing of p53 loss in sarcomagenesis. Cancer Res, 2011 71(11): p. 4040–7. [PubMed: 21512139]
27. Levy JMM, Towers CG, and Thorburn A, Targeting autophagy in cancer. Nat Rev Cancer, 2017 17(9): p. 528–542. [PubMed: 28751651]
28. Levy JM, et al., Autophagy inhibition improves chemosensitivity in BRAF(V600E) brain tumors. Cancer Discov, 2014 4(7): p. 773–80. [PubMed: 24823863]
29. Mulcahy Levy JM, et al., Autophagy inhibition overcomes multiple mechanisms of resistance to BRAF inhibition in brain tumors. Elife, 2017 6.
30. Ma XH, et al., Targeting ER stress-induced autophagy overcomes BRAF inhibitor resistance in melanoma. J Clin Invest, 2014 124(3): p. 1406–17. [PubMed: 24569374]
31. Eng CH, et al., Macroautophagy is dispensable for growth of KRAS mutant tumors and chloroquine efficacy. Proc Natl Acad Sci U S A, 2016 113(1): p. 182–7. [PubMed: 26677873]
32. Rosenfeldt MT, et al., p53 status determines the role of autophagy in pancreatic tumour development. Nature, 2013 504(7479): p. 296–300. [PubMed: 24305049]
33. Sousa CM, et al., Pancreatic stellate cells support tumour metabolism through autophagic alanine secretion. Nature, 2016 536(7617): p. 479–83. [PubMed: 27509858]
34. Poillet-Perez L, et al., Autophagy maintains tumour growth through circulating arginine. Nature, 2018 563(7732): p. 569–573. [PubMed: 30429607]
35. Honda A, et al., Potent, Selective, and Orally Bioavailable Inhibitors of VPS34 Provide Chemical Tools to Modulate Autophagy in Vivo. ACS Med Chem Lett, 2016 7(1): p. 72–6. [PubMed: 26819669]
36. Egan DF, et al., Small Molecule Inhibition of the Autophagy Kinase ULK1 and Identification of ULK1 Substrates. Mol Cell, 2015 59(2): p. 285–97. [PubMed: 26118643]

37. Kim KB, et al., Phase II study of the MEK1/MEK2 inhibitor Trametinib in patients with metastatic BRAF-mutant cutaneous melanoma previously treated with or without a BRAF inhibitor. J Clin Oncol, 2013 31(4): p. 482–9. [PubMed: 23248257]

38. White NJ, The treatment of malaria. N Engl J Med, 1996 335(11): p. 800–6. [PubMed: 8703186]

39. Ben-Zvi I, et al., Hydroxychloroquine: from malaria to autoimmunity. Clin Rev Allergy Immunol, 2012 42(2): p. 145–53. [PubMed: 21221847]

40. Di Veroli GY, et al., Combenefit: an interactive platform for the analysis and visualization of drug combinations. Bioinformatics, 2016 32(18): p. 2866–8. [PubMed: 27153664]

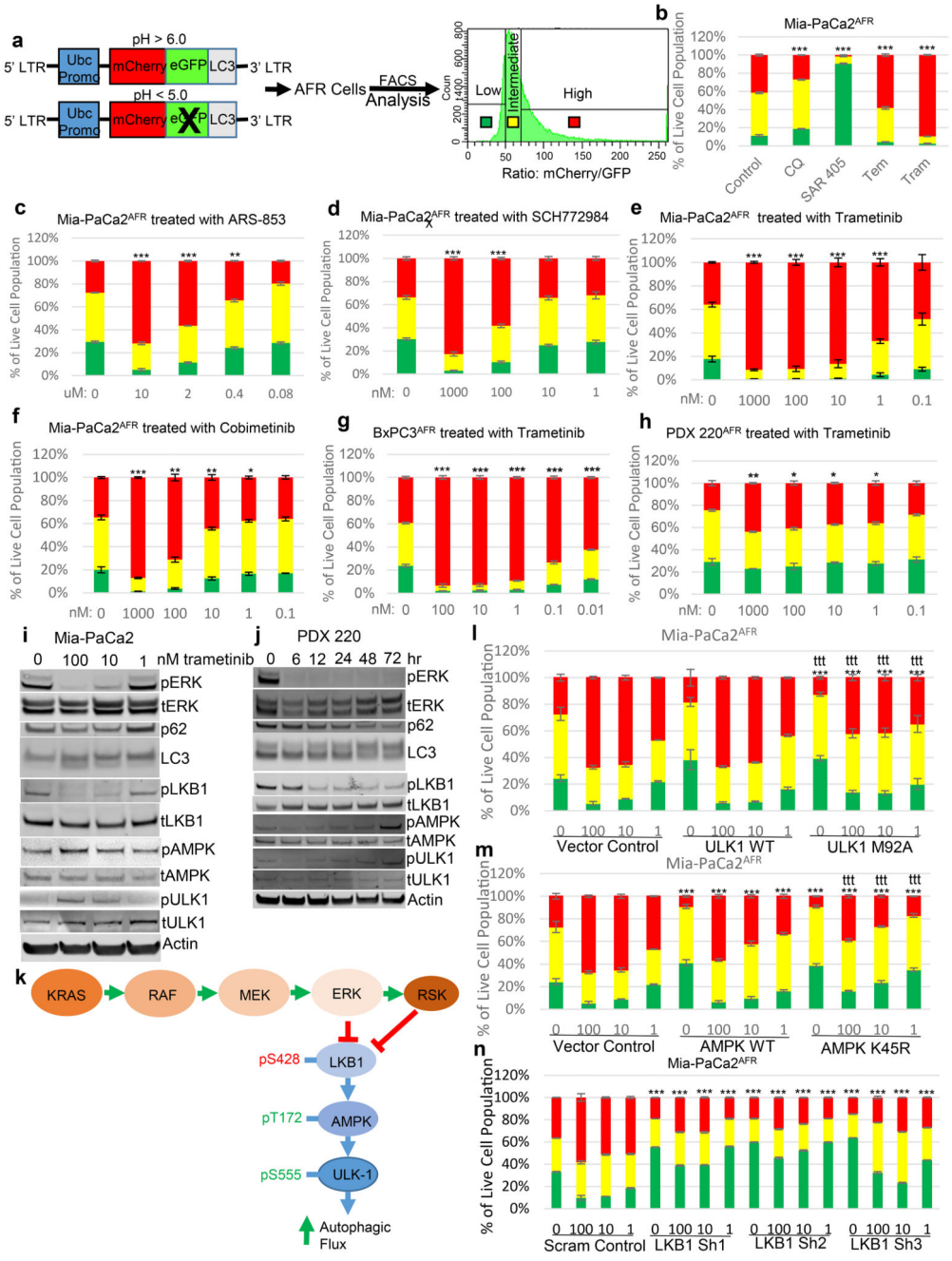

Figure 1. Inhibition of RAS→RAF→MEK→ERK signaling pathway induces autophagic flux (AF) in pancreatic cancer cells

a: Pancreatic cancer cells expressing an autophagic flux reporter (AFR) were generated by ectopic expression of a chimeric fusion protein comprised of mCherry-EGFP-LC3 in which the increased ratio of red:green fluorescence assessed by flow cytomtery is indicative of elevated AF.

b: Autophagic flux was assessed by flow cytometry in Mia-PaCa2^{AFR} cells following 48 hours treatment with various pharmacological inhibitors (CQ 20 uM or SAR-405 10 uM) or inducers (temsirolimus 10 uM or trametinib 100 nM) of autophagy. n=3; center values are

the mean; statistical testing was performed by two-sided t-test of control high (red) versus experimental high; ***p<0.001 vs. control (0 nM/uM). Error bars represent SD.

c-h: Mia-PaCa2^{AFR}, BxPC3^{AFR} or PDX220^{AFR} (derived from a human pancreatic cancer PDX) cells were treated for 48 hours with inhibitors of KRAS^{G12C} (ARS-853), ERK1/2 (SCH772984), or MEK1/2 (trametinib or cobimetinib) with autophagic flux assessed by flow cytometry. n=3; center values are the mean; statistical testing was performed by two-sided t-test of control high (red) versus experimental high; ***p<0.001, **p<0.01, *p<0.05 vs. control (0 nM/uM). Error bars represent SD.

i & j: Cell lysates prepared from Mia-PaCa2 treated with 1–100nM trametinib for 48 hours (a) or PDX220 derived cells treated with 100nM of trametinib over a time course (b), were analyzed by immunoblotting for the phosphorylation (p) or total (t) abundance of ERK1/2, p62, LC3, LKB1 (pS428), AMPK (pT172), ULK1 (pS555) or actin as indicated. Experiments were repeated three times with similar results.

k: Schematic model of the proposed mechanism by which inhibition of RAS→RAF→MEK→ERK signaling may elicit autophagic flux in pancreatic cancer cells.

l & m: Autophagic flux was assessed by flow cytometry in Mia-PaCa2^{AFR} cells transiently expressing exogenous ULK1 WT, ULK M92A (dominant negative) (d), AMPK WT, or AMPK^{K45R} (dominant negative) (e) and treated with 1–100nM of trametinib for 48 hours. n=3; center values are the mean; statistical testing was performed by two-sided t-test of matched treatment control high (red) versus matched dominant negative treatment high or matched treatment WT versus matched dominant negative treatment high; ***p<0.001 vs. matched treatment control; ^{ttt}p<0.001 vs. matched treatment WT. Error bars represent SD.

n: Autophagic flux was assessed by flow cytometry in Mia-PaCa2^{AFR} cells stably expressing shRNAs targeting LKB1 or scrambled control and treated with 1–100nM of trametinib for 48 hours. n=3; center values are the mean; statistical testing was performed by two-sided t-test; ***p<0.001 vs. matched treatment scrambled control. Error bars represent SD.

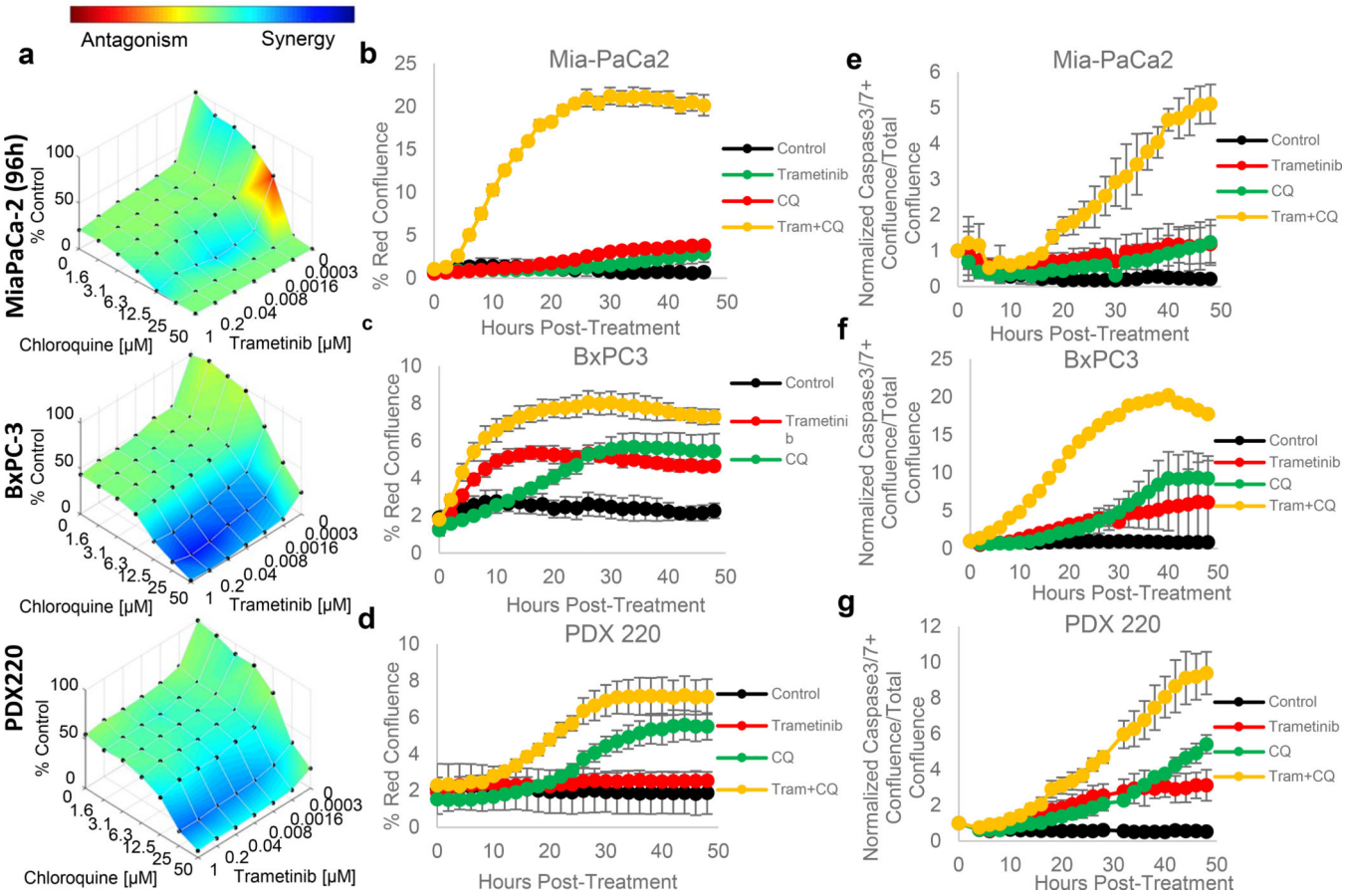

Figure 2. Trametinib and chloroquine are synergistically cytotoxic in vitro.

a: Mia-PaCa2, BxPC3 and PDX220 cells were treated for 48–96 as indicated with trametinib and chloroquine and analyzed for cell viability by ATPlite assay. Synergy graphs were generated utilizing Combenefit Software. Experiments were repeated 4 times with similar results.

b-d: Mia-PaCa2, BxPC3 and PDX220 cells were treated for 48 hours as indicated with vehicle (Control; DMSO), trametinib 100nM, chloroquine (CQ) 20μM or trametinib plus chloroquine and analyzed for cell viability by CytoxRed assay using an Incucyte Microscope. n=3; center values are the mean; statistical testing was performed by one-way ANOVA; $p<0.001$ for Tram+CQ vs. Control, CQ or trametinib in all experiments.

e-g: Mia-PaCa2, BxPC3 or PDX220 cells were treated for 48 hours as indicated with vehicle (Control; DMSO), trametinib 100nM, chloroquine 20μM or trametinib plus chloroquine and analyzed for apoptosis by Caspase-3/7 Green Apoptosis assay using an Incucyte Microscope. n=3; center values are the mean; statistical testing was performed by one-way ANOVA; $p<0.001$ for Tram+CQ vs. Control, CQ and Trametinib in all experiments.

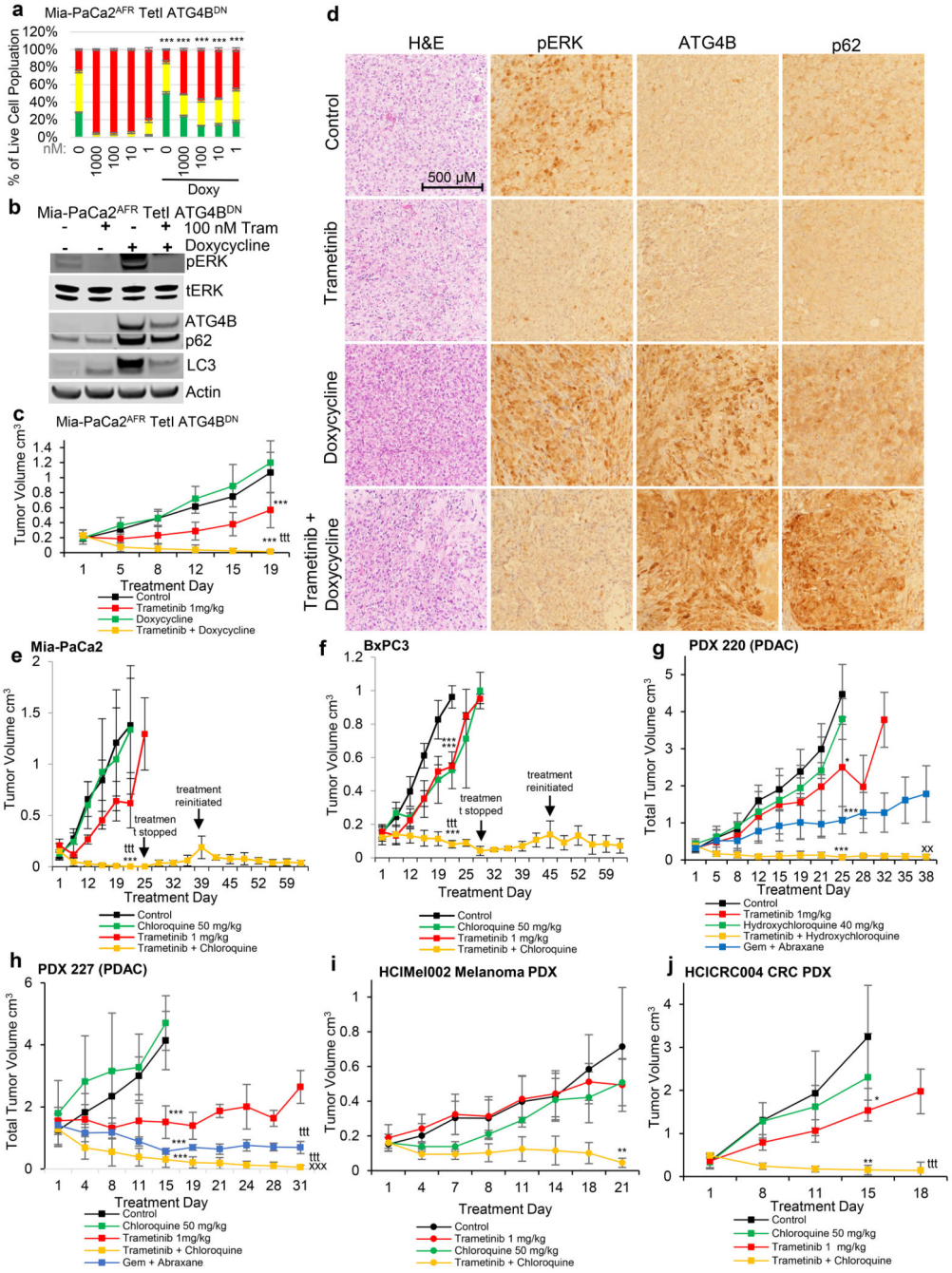

Figure 3. Tumor cell autonomous inhibition of autophagy cooperates with MEK1/2 inhibition to elicit regression of xenografted pancreatic tumors

a: Mia-PaCa2^{AFR} cells, engineered to express a doxycycline-regulated dominant-negative (DN) form of ATG4B (Mia-PaCa2^{AFR} TetI-ATG4B^{DN}) were treated with trametinib in the absence or presence of doxycycline with autophagic flux measured by flow cytometry. n=3; center values are the mean; statistical testing was performed by two-sided t-test of control high (red) versus experimental high; ***p<0.001 vs. trametinib treatment alone. Error bars represent SD.

b: Immunoblot analysis of the expression of the autophagy indicator proteins p62 and LC3 in Mia-PaCa2^{AFR} TetI-ATG4B^{DN} treated with trametinib, doxycycline (to induce ATG4B^{DN} expression) or both agents. This was repeated three times with similar results.

c: The growth of xenografted tumors of Mia-PaCa2^{AFR}/TetI-ATG4B^{DN} cells was assessed over 20 days in mice treated with: 1. vehicle (Control) n=11; 2. Trametinib n=11; 3. Doxycycline n=10 or; 4. the combination of both agents n=12. Center values are the mean; statistical testing was performed by two-sided t-test; ***p<0.001 vs. control; ^{ttt}p<0.001 vs. trametinib. Error bars represent SD.

d: Representative images of immunohistochemical analysis of sections of xenografted Mia-PaCa2^{AFR} TetI-ATG4B^{DN} tumors that were treated with 1. vehicle (Control), 2. trametinib; 3. doxycycline or; 4. the combination of both agents. Sections were stained with H&E or with antisera against pERK1/2, ATG4B or p62 as indicated. Scale bar is 500 μM located in the bottom right of the upper left panel and is consistent for all images.

e & f: The growth of tumor xenografts of Mia-PaCa2 (a) or BxPC3 (b) cells over ~60 days in mice treated with: 1. vehicle (Control); 2. trametinib (1mg/kg); 3. chloroquine (50mg/kg), or; 4. the combination of both agents at the aforementioned doses were assessed as indicated. Mia-PaCa2: control n=5, trametinib n=6, chloroquine n=5, combination of both agents n=4. BxPC3: n=6 for all treatment groups. Center values are the mean; statistical testing was performed by two-sided t-test; ***p<0.001 vs. control; ^{ttt}p<0.001 vs. trametinib. Error bars represent SD.

g & h: The growth of two pancreatic cancer patient derived xenografts (PDX220 or PDX227) in mice treated with: 1. vehicle (Control), 2. trametinib (1mg/kg), 3. hydroxychloroquine (40mg/kg in PDX220), chloroquine (50mg/kg in PDX227); 4. gemcitabine plus abraxane or; 5. the combination of trametinib plus CQ/HCQ at the aforementioned doses were assessed over ~30–40 days as indicated. PDX220: control n=6, trametinib n=5, hydroxychloroquine n=5, combination of both agents n=4, gemcitabine plus abraxane n=6. PDX227: n=5 for all groups except for gemcitabine plus abraxane n=6. Center values are the mean; statistical testing was performed by two-sided t-test; ***p<0.001, *p<0.05 vs. control; ^{ttt}p<0.001 vs. trametinib, ^{xxx}p<0.001, ^{xx}p<0.01 vs. gemcitabine plus abraxane. Error bars represent SD.

i & j: The growth of *NRAS*-mutated melanoma (HCI-Mel002) PDX or a *BRAF*-mutated colorectal cancer PDX (HCI-CRC004) was assessed over 18–21 days in mice treated with: 1. vehicle (Control), 2. trametinib (1mg/kg), 3. chloroquine (50mg/kg) or; 4. the combination of both agents at the aforementioned doses as indicated. HCI-Mel002: control n=5, trametinib n=5, chloroquine n=4, combination of both agents n=4. HCI-CRC004: n=5 for all groups except combination of both agents n=4. Center values are the mean; statistical testing was performed by two-sided t-test; **p<0.01, *p<0.05 vs. control; ^{ttt}p<0.001 vs. trametinib. Error bars represent SD.

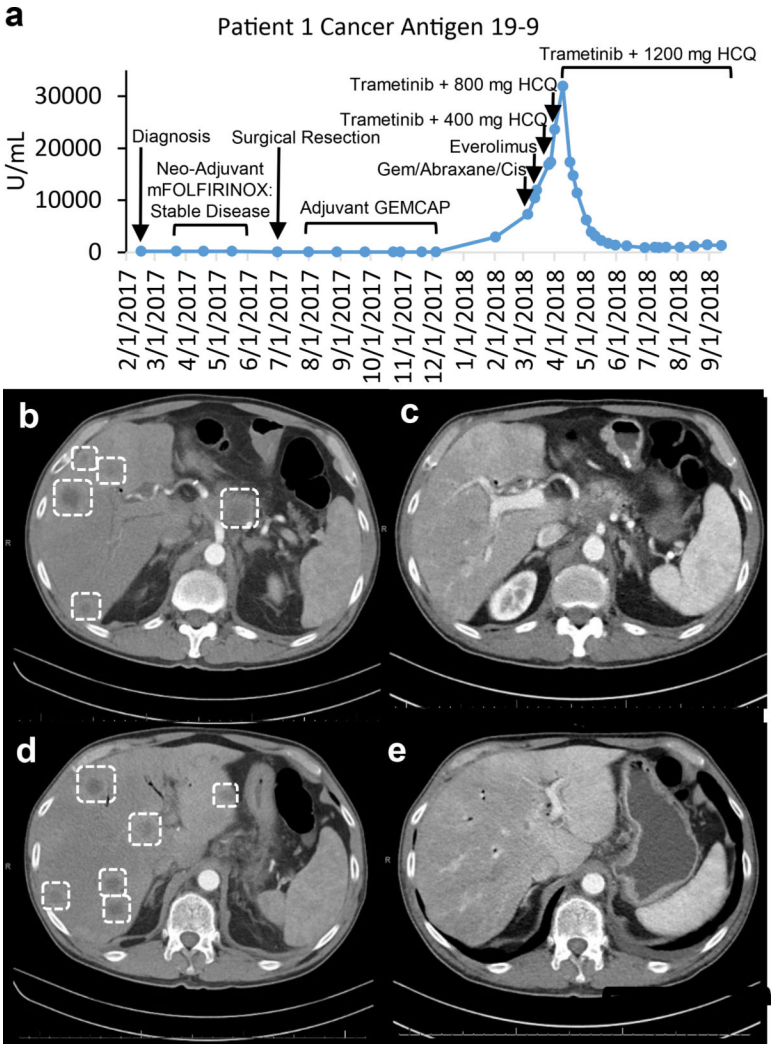

Figure 4. Treatment of a pancreatic cancer patient with trametinib plus hydroxychloroquine (T/HCQ) lead to a reduction in tumor marker cancer antigen 19–9 (CA19–9) and overall tumor burden.

a: The patient's blood-borne CA19–9 tumor marker was measured periodically throughout the the entire clinical course and is annotated with the dates and treatments administered. b, c, d & e: CT imaging 2 days after starting (b, d) the 2mg trametinib (q.d.) plus 1200mg (600mg b.i.d.) dosing of HCQ (which had been started with lower doses of HCQ two weeks previously) and two months post (c & e). The recurrent pancreatic bed lesion is dramatically reduced in size (comparing panel b to c), while the metastatic lesions in the liver are largely resolved (comparing panels b to c and d to e).